ELSEVIER

Effects in a climate model of slope tapering in neutral physics schemes

Anand Gnanadesikan *, Stephen M. Griffies, Bonita L. Samuels

*NOAA Geophysical Fluid Dynamics Laboratory, Princeton University, Forrestal Campus, 201, Forrestal Road,
Princeton, NJ 08540-6649, United States*

Abstract

In many global ocean climate models, mesoscale eddies are parameterized as along isopycnal diffusion and eddy-induced advection (or equivalently skew-diffusion). The eddy-induced advection flattens isopycnals and acts as a sink of available potential energy, whereas the isopycnal diffusion mixes tracers along neutral directions. While much effort has gone into estimating diffusivities associated with this closure, less attention has been paid to the details of how this closure (which tries to flatten isopycnals) interacts with the mixed layer (in which vertical mixing tries to drive the isopycnals vertical). In order to maintain numerical stability, models often stipulate a maximum slope S_{max} which in combination with the thickness diffusivity A_{gm} defines a maximum eddy-induced advective transport $A_{gm}*S_{max}$. In this paper, we examine the impact of changing S_{max} within the GFDL global coupled climate model. We show that this parameter produces significant changes in wintertime mixed layer depth, with implications for wintertime temperatures in key regions, the distribution of precipitation, and the vertical structure of heat uptake. Smaller changes are seen in details of ventilation and currents, and even smaller changes as regards the overall hydrography. The results suggest that not only the value of the coefficient, but the details of the tapering scheme, need to be considered when comparing isopycnal mixing schemes in models.

1. Introduction

Since its discovery in the late 1950s (Swallow, 1971) physical oceanographers have been extremely interested in the impact of the mesoscale eddy field on the large scale flow. It was quickly recognized that one important feature of the eddy field was that it would result in lateral tracer dispersion, and subsequent measurements (Ledwell et al., 1998) have shown that this dispersion occurs almost entirely along isopycnal surfaces (Redi, 1982). This mixing was incorporated into z-coordinate ocean models by Cox (1987), with later

---

refinements by Griffies et al. (1998). Additionally, numerical simulations (Rhines and Holland, 1979; Rhines and Young, 1982) suggested early that these eddies would also mix potential vorticity. Gent and McWilliams (1990) and Gent et al. (1995) developed a parameterization that aims to partially represent this process by diffusing thickness between isopycnals. They do so by including an eddy-induced advective term to the tracer equation which tends to drive isopycnals towards being horizontal, thus homogenizing the height of a layer bounded by two such isopycnals. Greatbatch and Lamb (1990) note that this effect can also be represented as a large eddy-induced vertical viscosity working on the mean shear. In most models, however, it is described in terms of the following mixing tensor (Griffies, 1998):

$$
\mathbf{J} = \begin{pmatrix}
A_{\mathrm{I}} & 0 & (A_{\mathrm{I}} - A_{\mathrm{gm}})S_x \\
0 & A_{\mathrm{I}} & (A_{\mathrm{I}} - A_{\mathrm{gm}})S_y \\
(A_{\mathrm{I}} + A_{\mathrm{gm}})S_x & (A_{\mathrm{I}} + A_{\mathrm{gm}})S_y & S^2 A_{\mathrm{I}}
\end{pmatrix}.
\tag{1}
$$

In this equation, A_{I} is the along isopycnal diffusion coefficient, A_{gm} is the thickness diffusion coefficient, and S_x and S_y are the isopycnal slopes in the x and y directions respectively and S is the magnitude of the isopycnal slope. The transport of any scalar property is then given by $\mathbf{F}_{\mathrm{C}} = -\mathbf{J} \cdot \nabla C$.

Significant attention has been paid to the value of the eddy diffusion coefficients A_{I} and A_{gm}, with various representations suggested by Visbeck et al. (1997), Held and Larichev (1996) and Griffies et al. (2005). Our own work has shown that the value of A_{I} in diagnostic models of ocean circulation can have important effects on the depth of the pycnocline (Gnanadesikan, 1999a), the lateral transport of heat (Gnanadesikan et al., 2003), the rate of global biological cycling (Gnanadesikan, 1999b; Gnanadesikan et al., 2002) and the uptake of anthropogenic tracers such as CO_2 and chlorofluorocarbons (Matsumoto et al., 2004). Work by Karsten and Marshall (2002) has discussed how eddies drive flow in the mixed layer, compensating some part of the Ekman flow so as to allow for a density balance. Ito et al. (2004) and Mignone et al. (2006) discussed how this could affect the uptake of anthropogenic carbon dioxide.

What happens as S becomes very large? Gerdes et al. (1991) and Gough (1997) noted that in models with isopycnal mixing alone, large values of isopycnal mixing coefficient could result in numerical instability and proposed that the isopycnal mixing coefficient needed to be tapered. Gough and Welch (1994) noted that the circulation in an idealized box was in fact sensitive to the value at which this tapering occurred. While Griffies et al. (1998) noted that stability could be maintained by avoiding the small angle approximation, this does not mean that the solutions produced by allowing large S are realistic. Oschlies (1999) for example notes that allowing large vertical diffusion coefficients in regions that are neutrally stratified (essentially allowing the mesoscale eddy parameterization to function as a vertical diffusion parameterization) resulted in systematically deep mixed layers. For this reason, he recommended tapering A_{I} to zero in regions of low stratification.

A different set of problems may be deduced for A_{gm}. Examination of (1) reveals that as discussed by a number of authors (McDougall, 1998; Killworth, 1998, 2001; Karsten and Marshall, 2002; Ferrari and McWilliams, 2006) it is possible to define a streamfunction Ψ^{eddy} for the mass transport associated with the eddy-induced flow. Insofar as the eddy driven flow in the interior is adiabatic and is therefore driven along isopycnal surfaces it is possible to isolate some portion of the eddy-driven flow for which

$$
\Psi^{\mathrm{eddy}} = \frac{-\overline{w'\rho'}}{\overline{\rho_y}} = \frac{\overline{v'\rho'}}{\overline{\rho_z}}
\tag{2}
$$

such that Ψ^{eddy} satisfies the equation

$$
-\Psi^{\mathrm{eddy}}_z \overline{\rho_y} + \Psi^{\mathrm{eddy}}_y \overline{\rho_z} = \overline{v'\rho'}_y + \overline{w'\rho'}_z
\tag{3}
$$

If one makes the assumption that $\overline{v'\rho'} = -A_{\mathrm{gm}}\overline{\rho}_y$ then $\Psi^{\mathrm{eddy}} = A_{\mathrm{gm}}S_y$. This is essentially the form in which the eddy-induced transport is implemented in the scheme of Gent and McWilliams (1990). However, such an implementation results in problems when the slope becomes large. As discussed in a recent manuscript by Ferrari and McWilliams (2006), a number of different solutions have been proposed to keep the velocity from reaching unphysical values within the mixed layer. In the Modular Ocean Model, Version 3 (Pacanowski and Griffies, 1999), the slope was tapered to zero at the edge of the mixed layer. In the Modular Ocean Model, Version 4 (Griffies et al., 2003) we have chosen a different scheme, in which

$$\Psi^{\mathrm{eddy}}(z) = \Psi^{\mathrm{eddy}}(z=h)\frac{z+h}{\eta+h} \qquad (4)$$

where h is the depth at which the slope becomes greater than $S_{\max}$ and η is the free surface height. This is essentially identical to the form suggested by Karsten and Marshall (2002) and Ferrari and McWilliams (2006) in the absence of a transition zone. However, in realistic situations, spreading out the eddy flux like this does not eliminate all associated problems. A_{gm} is often taken to be of order hundreds or even thousands of $\mathrm{m}^2\,\mathrm{s}^{-1}$ (Davis, 2005). Even if the isopycnal slopes below the mixed layer base are only of order 0.01, the resulting eddy flux can be of order $10\,\mathrm{m}^2\,\mathrm{s}^{-1}$. The Ekman flux within the mixed layer is only of order $1\,\mathrm{m}^2\,\mathrm{s}^{-1}$. In other words, without some sort of tapering scheme, $\Psi^{\mathrm{eddy}}(z=h)$ may still be large enough so that it produces a flux many times larger than the Ekman flux.

In the GFDL coupled climate model, this problem was dealt with by setting a maximum value $S = S_{\max}$ within the GM scheme, effectively limiting the maximum magnitude of Ψ^{eddy} to $A_{\mathrm{gm}}S_{\max}$. As illustrated in Fig. 1, changing $S_{\max}$ can have an effect on the eddy-driven circulation. The plot shows the result of two one-day runs initialized from the end of a 100 year coupled simulation in which $S_{\max} = 1/500$ (described in more detail in Section 2). In the left-hand panel $S_{\max}$ is kept at $1/500$. In the other it is instantaneously increased to $1/100$. Because of the short duration of the runs, the density structure driving the GM overturning is essentially identical. As a result the overturning streamfunction below the mixed layer is essentially the same in the two simulations. The overturning in the mixed layer, however, is substantially different. With the high value of $S_{\max}$ the high slopes within the mixed layer result in an overturning that transports much more mass than the deep overturning. This is somewhat disconcerting, as the GM parameterization is intended to represent the restratification associated with low-mode baroclinic eddies, not necessarily that associated with small-scale mixing within the mixed layer. It is also striking in that model descriptions are not always careful to identify this parameter or to discuss the way in which the isopycnal slopes are tapered. Note that the zero lines for
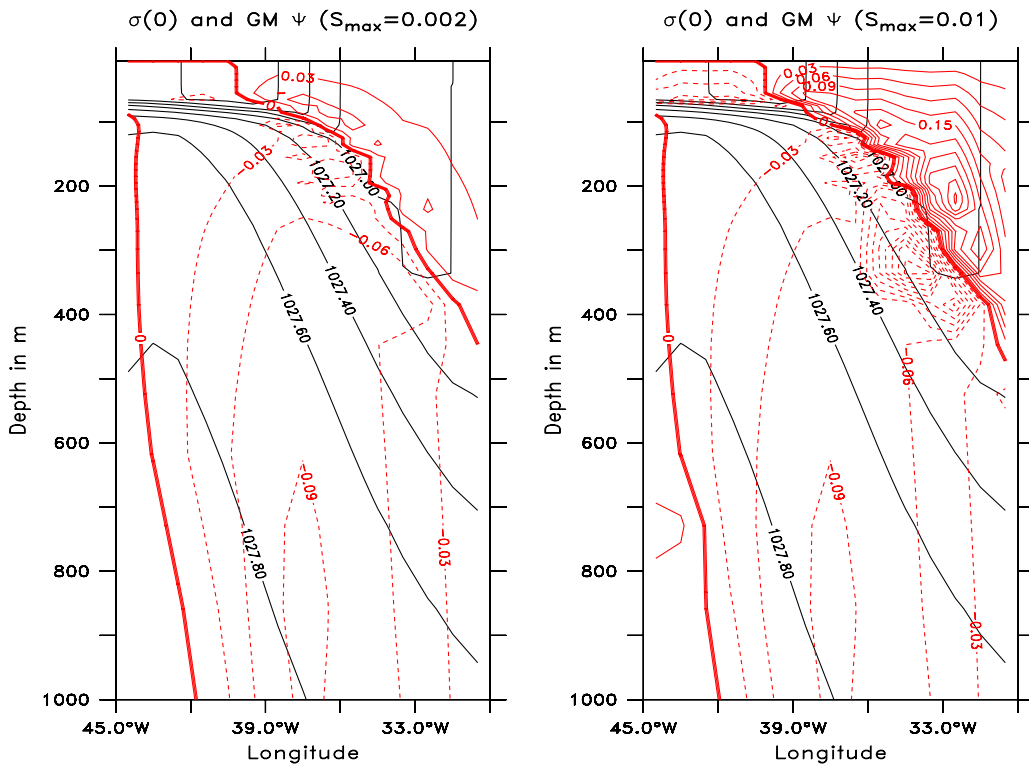

Fig. 1. Difference in eddy driven overturning (Sv) at a single latitude from changing $S_{\max}$. Black lines represent the potential density referenced to the surface, red lines the overturning in Sv.

overturning are essentially the same in the two models, so that the direct impact of changing S_{max} on the overturning is much more important than the indirect effect of changing the location of the transition layer.

Since the overturning shown in Fig. 1 moves light water over dense water one would expect a higher value of S_{max}, (all else being equal) to increase the rate of restratification, causing a stronger eddy-induced heat transport, shallower mixed layers, less deep ventilation and increased SSTs during the summer months. In a coupled system, however, feedbacks may either amplify or damp the effects of changing S_{max}. The purpose of this paper is to examine how big the changes implied by Fig. 1 actually are in a realistic simulation. While we recognize that different coupled models, with different parameterization of, for example, cloud feedbacks may yield different results, our purpose is to identify processes that are particularly sensitive to S_{max} and those which are insensitive. The models used are described in more detail in Section 2. Section 3 describes the results and Section 4 concludes this paper.

2. Simulation description

We present two runs of the GFDL coupled climate model CM2.1. This model uses the finite-volume core atmosphere of Lin (2004) and the atmospheric physics packages are documented in a paper by the GFDL Global Model Atmospheric Development Team (2004). The ocean model is the Modular Ocean Model Version 4 (Griffies et al., 2003) configured as described in Griffies et al. (2005). Gnanadesikan et al. (2006) analyze the overall circulation in the 1990 control run of this model, which has relatively low drifts in upper ocean hydrography and reasonable values for the transports of many key currents. The reader is referred to these publications for details of the model formulation which is outlined below.

The ocean model consists of a fifty-level model with a longitudinal resolution of 1° and a latitudinal resolution varying between 1° in the extratropics and 1/3° on the equator. The model uses an explicit free surface with real freshwater flux (Griffies et al., 2001), has a mixed layer parameterization (Large et al., 1994), and incorporates such numerical innovations as anisotropic lateral viscosity (Large et al., 2001), a sophisticated advection scheme for tracers, partial bottom cells so that topography is relatively independent of vertical resolution (Pacanowski and Gnanadesikan, 1998), and a crude representation of the bottom boundary layer.

The model is initialized from a one-year ocean-only run, which is itself initialized from the World Ocean Atlas 2001 (Conkright et al., 2002). It is then spun up without flux adjustments. Radiative forcings due to well-mixed greenhouse gasses and aerosols are held at 1990 levels. We present solutions from the first 100 years of the simulation. While this is not long enough for the deep ocean to come into balance, it is long enough to see very significant changes in the wind-driven thermocline. As documented in Gnanadesikan et al. (2006) patterns of RMS temperature and salinity errors in the upper 1500 m are well established after only 60 years of simulation. In general, errors relative to observations and differences between the models are computed as averages from years 40 to 100 of the simulation.

We present two simulations-one in which $S_{max} = 1/500$ as in Delworth et al. (2006) and Gnanadesikan et al. (2006) and one in which $S_{max} = 1/100$. As both runs have modern greenhouse gas concentrations, they are not in radiative balance and have a mean uptake of around 1 W m^{-2}, the consequences of which will be explored towards the end of the Section 3.

3. Results

One of the first questions in looking at models of ocean circulation is what surface fluxes drive the model. Fig. 2 shows the annual-mean net flux of zonal momentum, heat, and freshwater in the two simulations. The two curves lie right on top of each other at all latitudes. The maximum zonally averaged differences in wind stress are only 0.004 Pa. The maximum zonally averaged difference in heat flux is 8.5 W m^{-2} with the mean absolute difference being only 1.8 W m^{-2} and the mean absolute difference in water flux is only about 4 cm/yr. These differences are much smaller than those seen between, for example, the different versions of the GFDL coupled model. Our results suggest that changing S_{max} is unlikely to be a means of fixing strong biases in Southern winds such as those reported by Russell et al. (2006).

Despite the fact that these changes in fluxes are small, there are still some surprisingly large changes in the surface properties of the ocean. As seen in Fig. 3, increasing S_{max} produces a complicated pattern of temper-
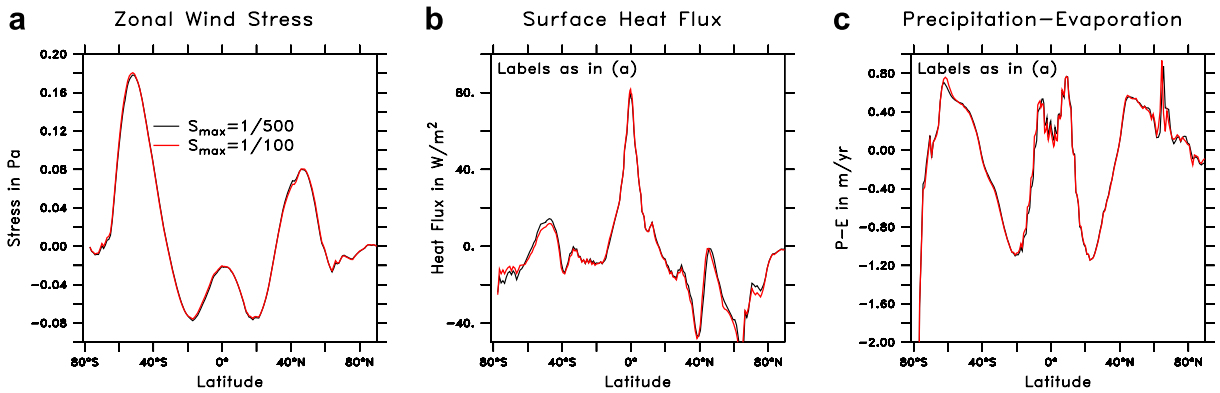
Fig. 2. Zonally averaged fluxes of (a) zonal momentum in Pa, (b) heat flux in W/m² and (c) net water flux (precipitation–evaporation) in m/yr. As can be seen from these plots, changing S_{max} has a very small impact on the air–sea fluxes.
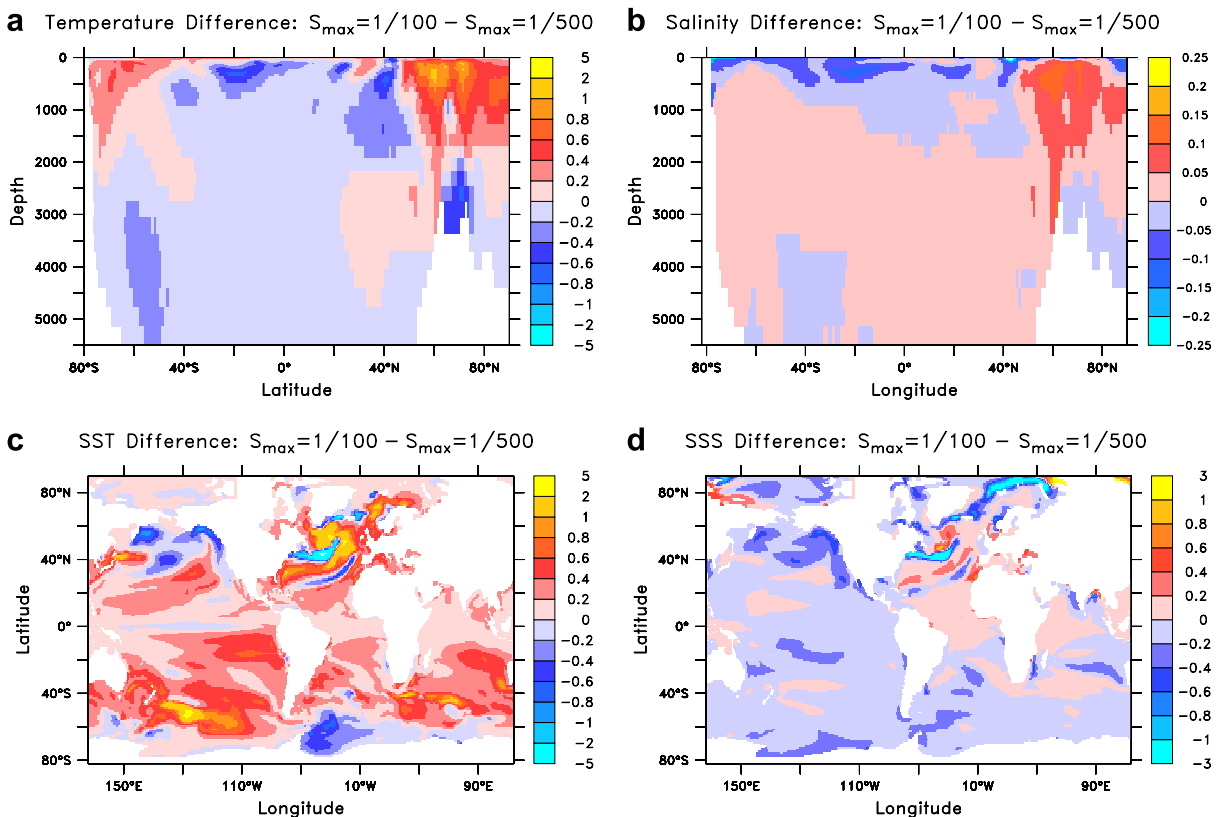

Fig. 3. Changes in mean hydrographic structure resulting from changes in S_{max}. All differences are the result of increasing S_{max} from 1/500 to 1/100. (a) Zonally averaged temperature difference in °C. (b) Zonally averaged salinity difference in PSU (note reduced scale relative to other plots) (c) Sea surface temperature difference in °C. (d) Sea surface salinity difference in PSU.

ature change. In the tropics, it acts to warm the surface and cool the subsurface. In the northern mode water formation regions, it acts to warm the surface and subsurface. The subpolar gyres in the North Pacific and Atlantic show very different signals. The North Pacific surface becomes cooler and fresher, consistent with its becoming more stratified. By contrast in the North Atlantic the subpolar gyre shifts southward (Fig. 4) and intensifies in the Labrador Sea. On the one hand, this means that more warm salty, surface water is drawn into this region, thus enhancing the formation of Labrador Sea Water. On the other hand, the movement of
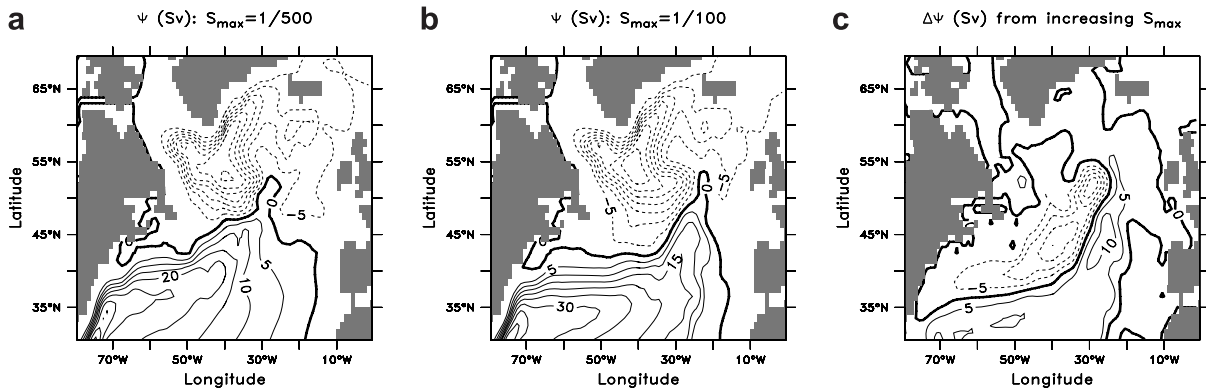
Fig. 4. Horizontal streamfunction Ψ(Sv) in the North Atlantic. Positive values denote clockwise circulation, negative anticlockwise. (a) For base case of $S_{max} = 1/500$. (b) For case where S_{max} is increased to 1/100. (c) Difference between the two cases.

the gyre boundary southward means that cold, fresh subpolar water extends too far to the south off of Newfoundland.

While these changes in surface properties are significant, the changes in interior hydrography are much more subtle. One diagnostic that was used to evaluate the CM2 models during the development process is the RMS error over the top 1500 m. As seen in Fig. 5 the differences in RMS error between the two models
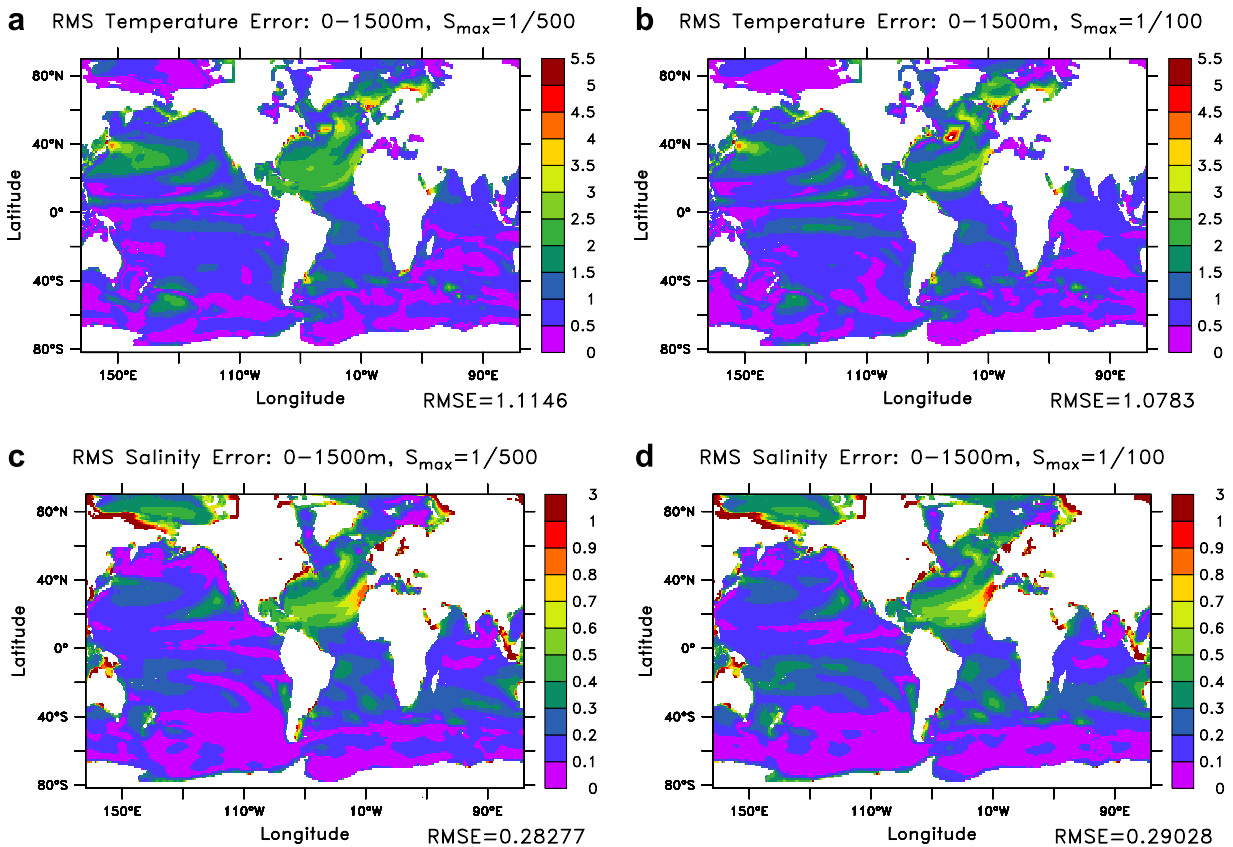

Fig. 5. RMS Error over top 1500 m for two values of S_{max}. Note that the differences are very small and the patterns very similar, with the exception of the North Atlantic. (a) Temperature, $S_{max} = 1/500$. (b) Temperature, $S_{max} = 1/100$. (c) Salinity, $S_{max} = 1/500$. (d) Salinity, $S_{max} = 1/100$.

are extremely subtle. Increasing S_{max} produces a small reduction in the overall temperature error but a 5% increase in the overall salinity error. Moreover, it increases the errors off of Newfoundland in the North Atlantic Current region – informally christened "the blue spot of death" by members of the GFDL coupled model development team. In the real world, the North Atlantic Current skirts the Grand Banks in this region and large temperature and salinity contrasts are seen between subtropical and subpolar waters. If the North
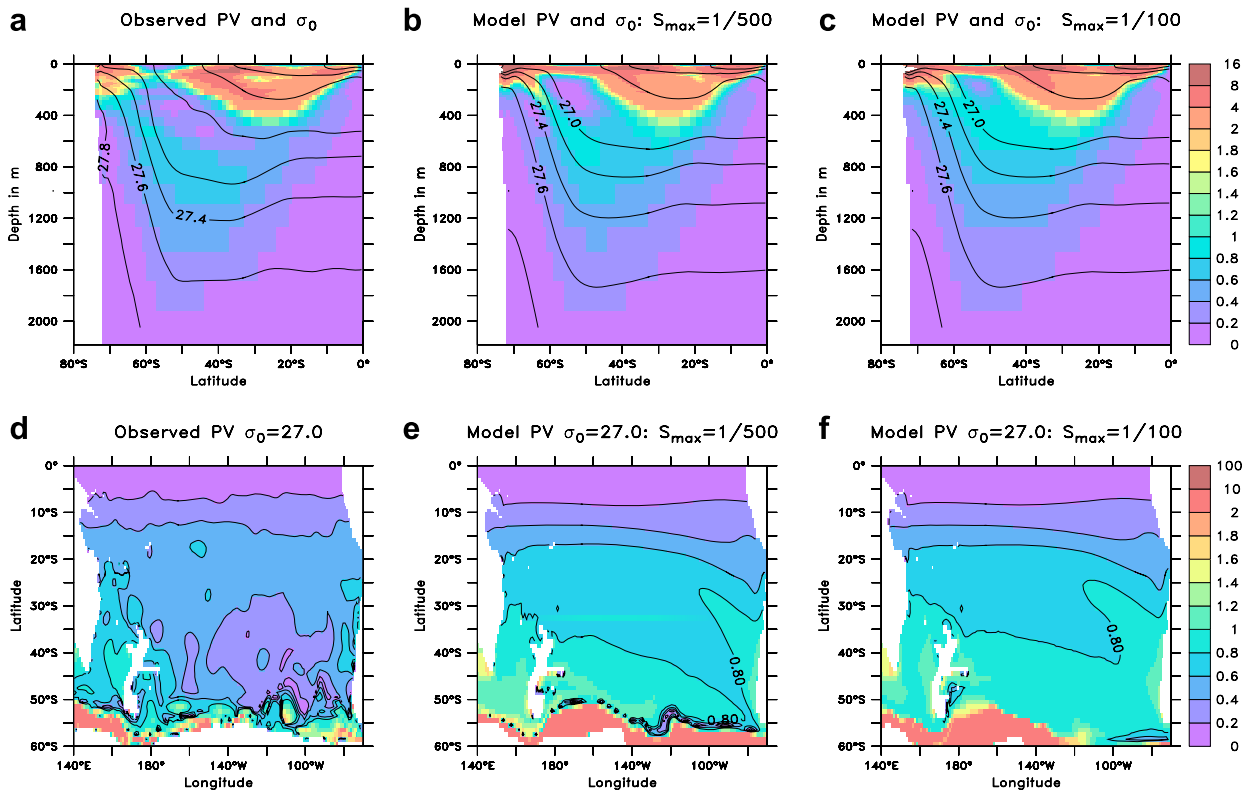

Fig. 6. Planetary geostrophic potential vorticity and potential density in the Southeast Pacific. Top row shows a cross section averaged from 120°W to 80°W, bottom row the distribution along the $\sigma_0 = 27.0$ surface. Potential vorticity is $\frac{f}{\rho}\frac{\partial\rho}{\partial z}$ in units of 10^{-10} m^{-1} s^{-1}. (a and d) From observations (b and e) coupled model with $S_{max} = 1/500$. (c and f) Coupled model with $S_{max} = 1/100$.
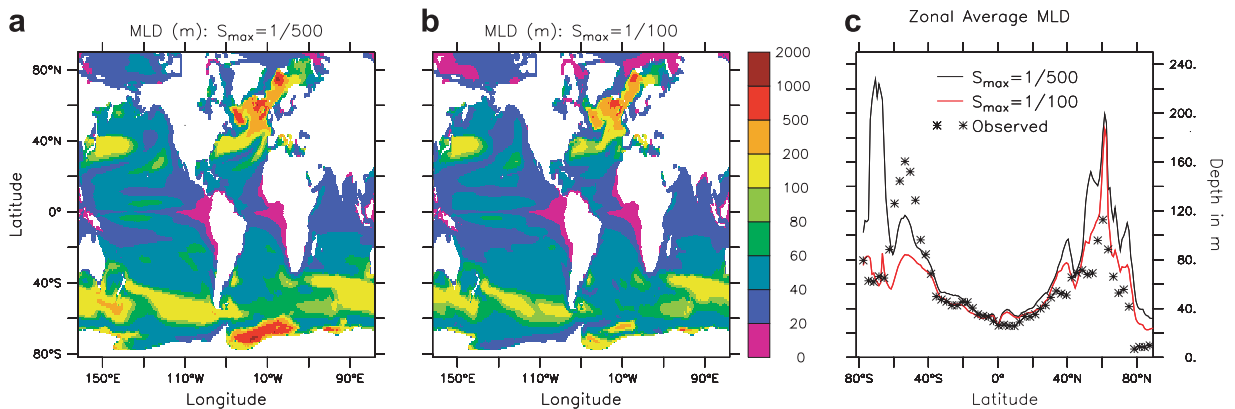

Fig. 7. Mixed layer depths in the two models compared with data. (a) Annual mean mixed layer depth in m in model with $S_{max} = 1/500$. (b) Annual mean mixed layer depth when S_{max} is increased to 1/100. (c) Zonal average compared with data.

Atlantic Current is slightly shifted, surface temperature biases of up to 10 °C may be found in a few points. In the current case, we find that increasing S_{max} increases the maximum local temperature error in this region from 7.7 to 8.7 °C. Reducing this error below 10 °C was one major goal of our model development effort as part of the IPCC process. While this seems to favor a lower value of S_{max}, it is likely that changes in S_{max} are likely compensating for other model deficiencies, such as the inability to resolve flows along the shelf to the south of Newfoundland. The global RMS SST errors are essentially the same for the two models (1.20 for the low S_{max} run and 1.23 for the high S_{max} run).
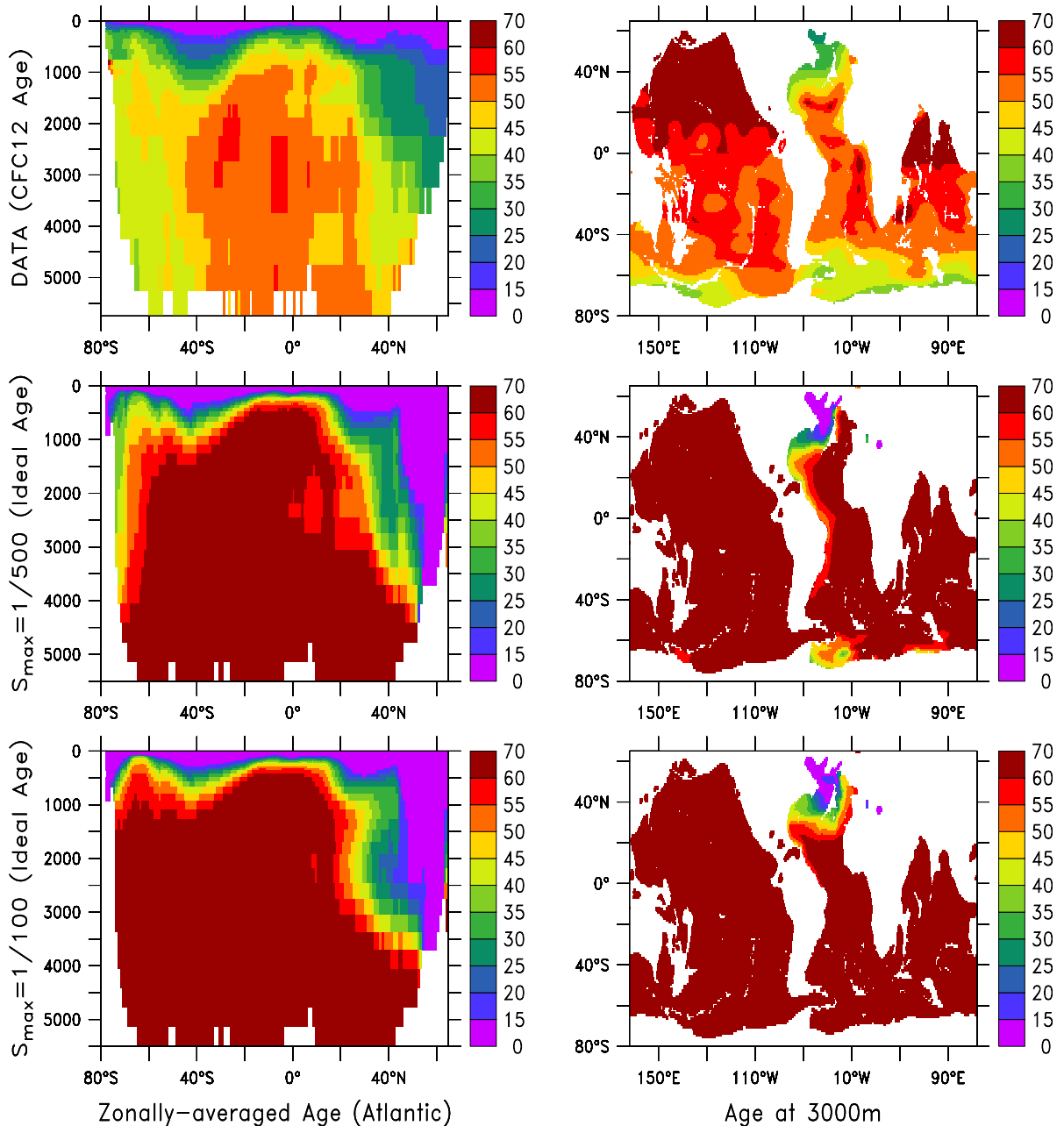

Fig. 8. Age in years in the Atlantic sector (left column) and at a depth of 3000 m (right column). Observations are CFC12 age (top row, in years), model output is ideal age. $S_{max} = 1/500$ run is shown in the middle row and $S_{max} = 1/100$ in the bottom row. Note that the higher value of S_{max} essentially eliminates Southern Ocean convection.

RMS temperature and salinity errors are important because they are used by model developers as metrics of how well the model is performing. Moving to the Southern Hemisphere, we find that a more careful examination of fields such as the potential vorticity structure (Fig. 6) is required to isolate differences. In the Southeast Pacific the potential vorticity (computed as $f*N^2/g$ using σ_0) is high near the surface and between the 27.2 and 27.4 isopycnal surface. In between, we find a band of low potential vorticity associated with the Subantarctic Mode Water. This low potential vorticity band is significantly attenuated in the case with $S_{max} = 1/500$ and has an even smaller extent in the run with $S_{max} = 1/100$. The effect of this is even more clearly seen when looking along the $\sigma_0 = 27.0$ surface (Fig. 6d–f). The data shows a pool of low potential vorticity water with
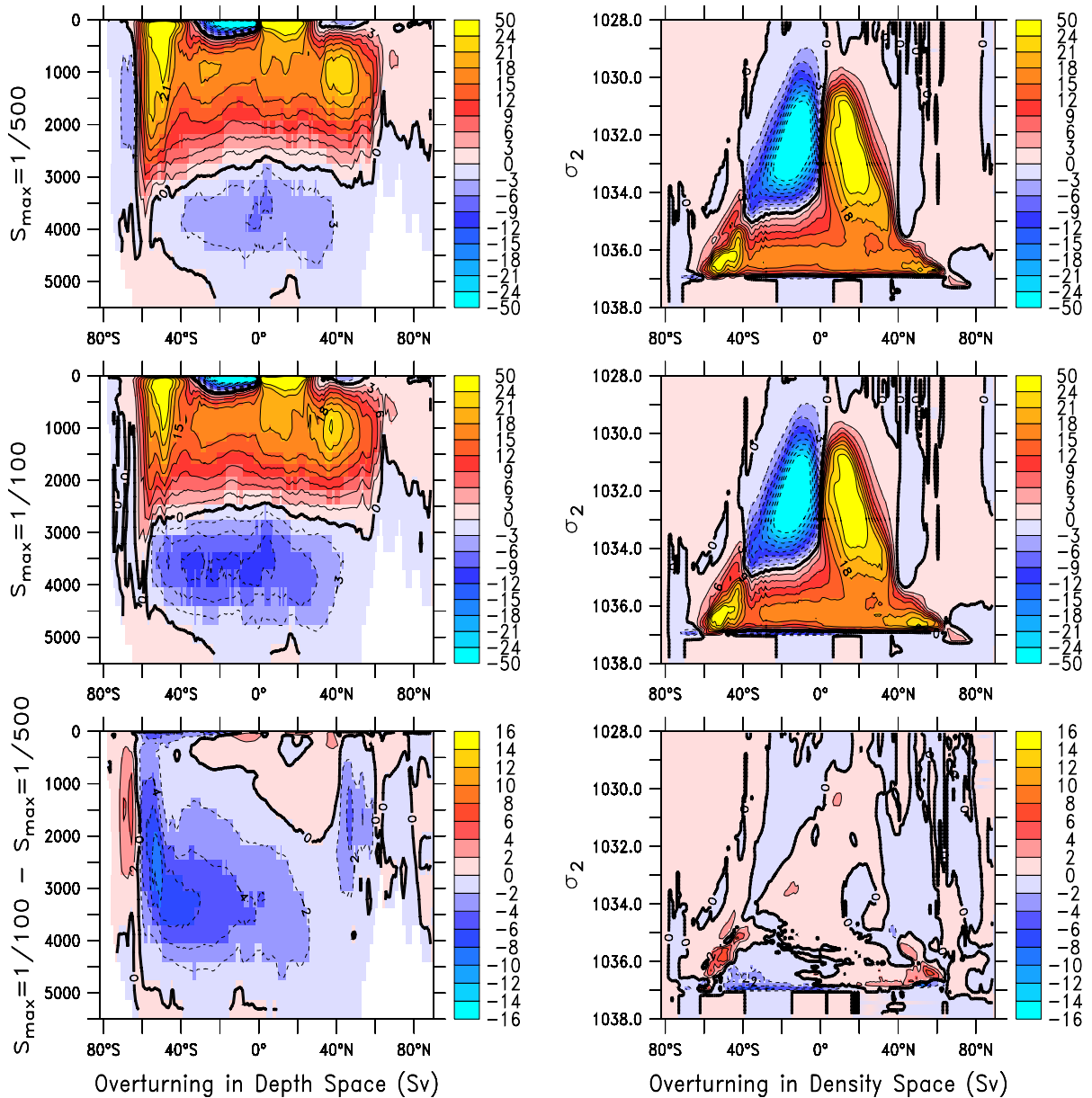

Fig. 9. Overturning streamfunction in Sv in the two models. Left-hand column shows overturning in depth space, right-hand column shows overturning in density space. Top row shows runs for $S_{max} = 1/500$ middle row for $S_{max} = 1/100$ and the bottom row the consequence of increasing S_{max}.

values less than 0.4×10^{-10} m^{-1} s^{-1} throughout much of the Southeast Pacific. In the case with $S_{max} = 1/500$ this area is limited to a narrow band. In the case with $S_{max} = 1/100$, the pool has vanished entirely.

The reduction in the extent of the pool of low PV water reflects the fact that increasing S_{max} causes the mixed layer to become shallow. This is clearly seen in Fig. 7, which compares the mixed layer depth to estimates made from the World Ocean Database 1998 (Levitus et al., 1998) using the methodology of (Monterey and Levitus, 1997). The observations are low in the tropics, and high in the northern extratropics and in the mode water formation region in the Southern Ocean. The baseline model with $S_{max} = 1/500$ has relatively deep mixed layers in the northern hemisphere but fails to capture the deep Southern Hemisphere mixed layers, instead opening up a convective region near the Antarctic margin. Increasing S_{max} essentially removes this region altogether, leaving mixed layer depths too shallow throughout the Southern Hemisphere.

The reduction in Southern Ocean mixed layer depths has important implications for the vertical exchange in this region. A field that shows this very clearly the ideal age. Ideal age is a measure of the time since a parcel was last at the surface. It is well-defined in a model context, but is more difficult to estimate from observations. Fig. 8 shows the ideal age in the two models compared with the age estimated using CFC12. The CFC12 age corresponds to the date before the present when water with the observed concentration of CFC12 (taken from the gridded dataset of Willey et al., 2004) would have been in equilibrium with the surface. The CFC12 age (top row) reveals that there is significant ventilation of the Southern Ocean, with significant levels of CFC throughout the Circumpolar region. That this is accomplished by downslope flow along the margin is suggested by the low observed values in CFC age there. By contrast the bulk of ventilation in the CM2.1 model occurs in the middle of the Weddell Sea. This is a frequent occurrence in ocean simulations, as this region is close to being unstable to cabelling. As described by Winton et al. (1998) level-coordinate models have significant difficulties resolving downslope flows. The CM2.0 model exhibits neither pathway of ventilation. In order to properly simulate biogeochemical cycling, we decided to accept an unrealistic pathway of deep ventilation in the Southern Ocean over no ventilation at all.

The changes in ventilation seen in the ideal age are not what one would expect from looking at the overturning streamfunction (Fig. 9). Increasing S_{max} does result in a decrease in the total amount of deep upwelling occurring in the Southern Ocean (as might be expected from previous work). However, it also seems to produce a more vigorous AABW overturning cell. A more careful examination of the overturning in density
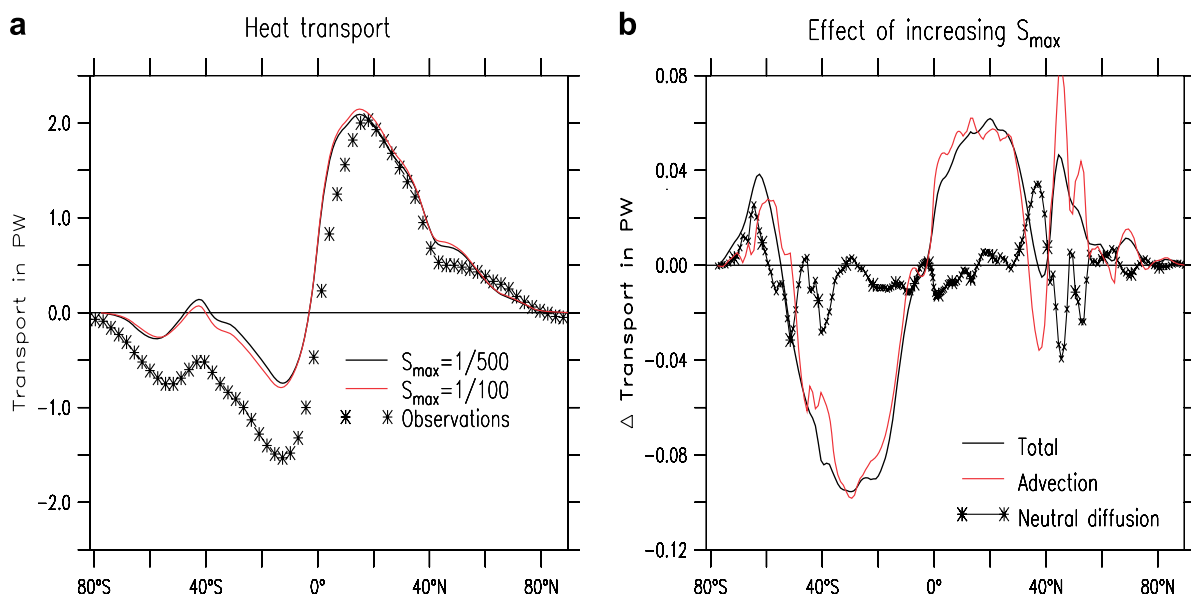

Fig. 10. Lateral transport of heat in the models. (a) Models compared with observationally-inferred transport by Trenberth and Caron (2001). (b) Effect of increasing S_{max} on heat transport broken into total effect (solid), effect due to mean advection (dashed) and lateral diffusion (solid + stars).

space, however shows that the apparently large changes in depth space are not matched by similar changes in density space and thus tend to reflect changes in the locations of flows rather than major changes in the magnitudes of watermass transformation (though there is some hints of an increase in Labrador Sea Water formation seen in density space – though not in depth space).

Because the changes in watermass formation are relatively small, we would expect the changes in lateral heat transport to be relatively small. This is in fact the case. As seen in Fig. 10a, the difference between the two models is much smaller than that between the models and the observationally inferred heat transport of Trenberth and Caron (2001). The maximum differences are seen in the Southern Ocean, amounting to about 0.12 PW. This difference arises almost entirely from the mean advective transport rather than the lateral diffusive transport (Fig. 10b). The impact of changing S_{max} on lateral heat transport is thus indirect rather than direct.
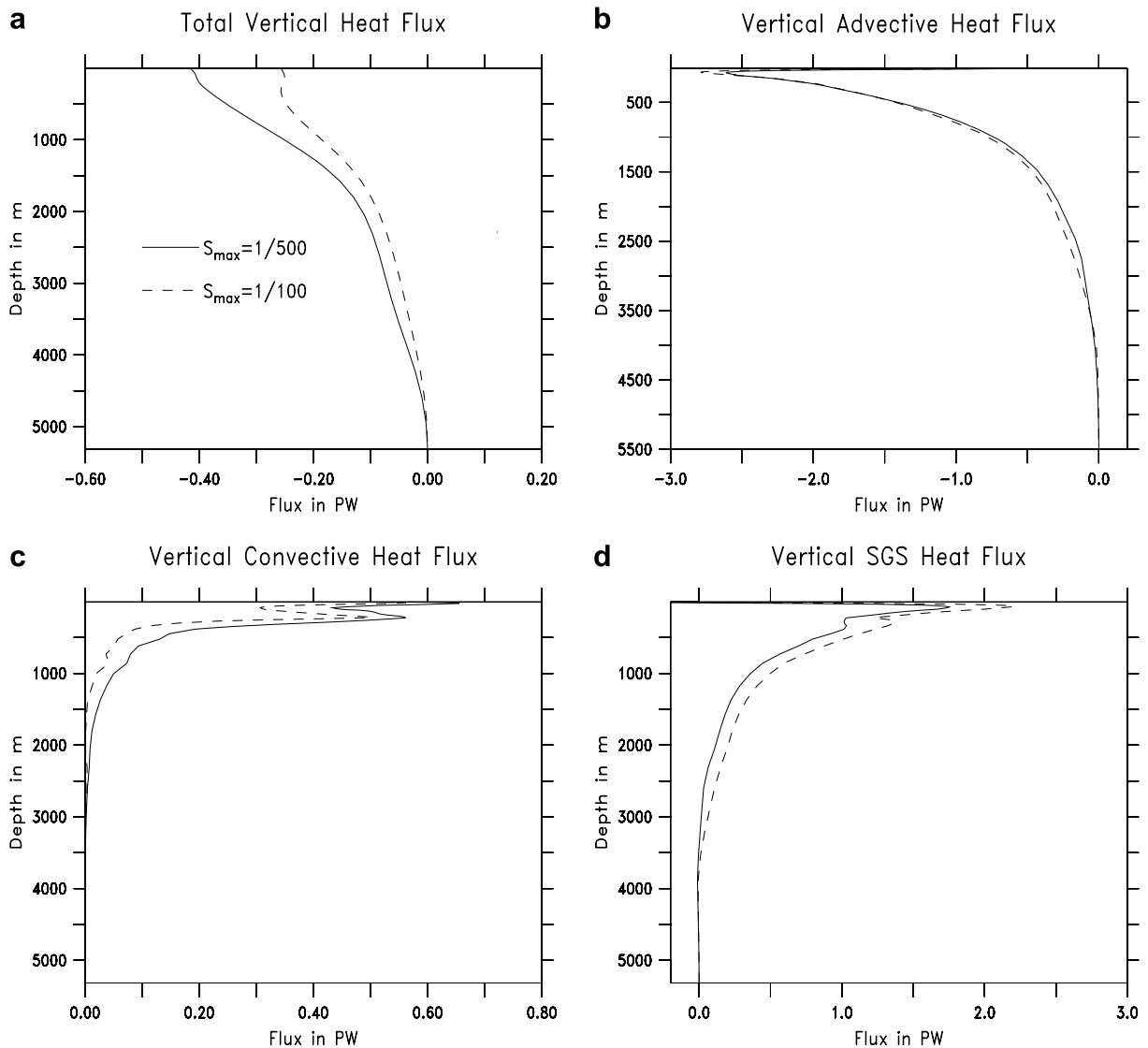

Fig. 11. Vertical transport of heat in PW due to various processes. Run with $S_{max} = 1/500$ is shown with solid lines, $S_{max} = 1/100$ with dashed lines. (a) Total heat transport. (b) Heat transport associated with vertical advection alone. (c) Vertical heat transport associated with convective adjustment. (d) Vertical heat transport associated with all other subgridscale processes.

The vertical heat transport, by contrast, shows more of an impact of changing S_{max}. As discussed in Gregory (2000) and Gnanadesikan et al. (2005) the dominant budget in realistic ocean circulation models involves downward advection of heat by the mean flow and upward transport of heat by convection and subgridscale processes like turbulent diffusion and eddy induced transport. The fact that the eddy induced transport of heat is actually upwards (the reverse of what would be expected from a simple diffusive closure) is largely due to the Gent–McWilliams parameterization moving warm water upwards in the tropics and cold water downwards in the poles. Gnanadesikan et al. (2005) uses the fact that the vertical advection of buoyancy is downwards in two realistic ocean-only models to argue that winds are primarily responsible for driving the ocean circulation.

The general picture painted by these papers is seen in our coupled models as well, as shown in Fig. 11. Interestingly, increasing S_{max} results in a significant change in the net heat flux into the ocean in this model. The baseline model has surface heat flux of 0.41 PW into the ocean (around 1.2 W m²), while the run $S_{max} = 1/100$ has a total heat flux of 0.26 PW. Thus, changing the value of S_{max} can have a significant effect on the total heat balance of the model of approximately 0.5 W m^{-2}. This is a significant fraction of the greenhouse gas forcing at present day- and illustrates that while the exact value of S_{max} may not be of first-order importance for the mean simulation, it has important implications for heat balance.

Further examination of Fig. 11 allows us to identify the processes responsible for changes in the heat uptake. The vertical heat transport in the models is relatively close below about 1000 m. Above this depth increasing S_{max} results in a decrease in the vertical convective heat flux of between 0.06 and 0.23 PW, which is more than compensated by an increase in the upward subgridscale heat flux of 0.15–0.45 PW. Below 1000 m the increase in vertical subgridscale heat flux is balanced not only by a decrease in convection, but by an increase in the downward vertical advective transport of heat.

Despite the fact that the zonal mean fluxes of heat and freshwater are almost identical in the two models, there are a few locations where a significant differences in mean climate are seen. One of these which is related
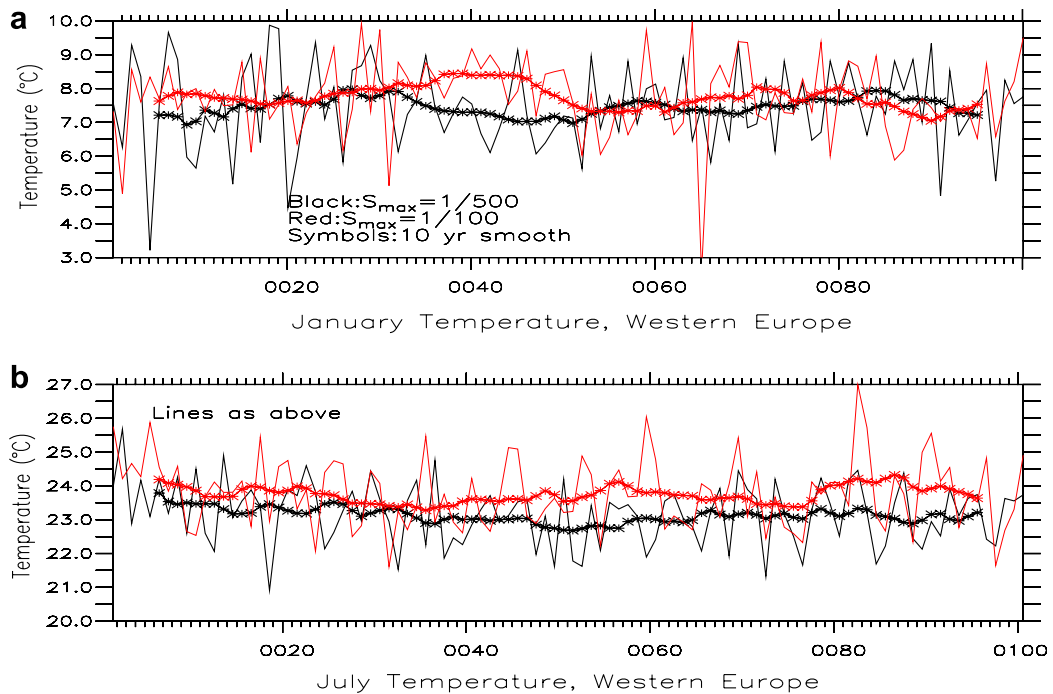

Fig. 12. Atmospheric temperature at 2 m averaged from 10 W–30E and 30–50N (basically corresponding to Western Europe). Black lines show baseline simulation with $S_{max} = 1/500$, red lines the perturbation simulation with $S_{max} = 1/100$ and symbols show a 10-year running mean. (a) January temperatures. Although the case with $S_{max} = 1/100$ appears to be a little warmer, it is far from clear that this is significant given the overall variability over a range of time scales. (b) July temperatures. The $S_{max} = 1/100$ simulation is warmer by about 0.5 °C and shows a clear separation from the baseline case.

to the shift in the North Atlantic gyre circulation (Fig. 4) which results in a warming in the northeastern Atlantic. Fig. 12 shows the temperatures over Western Europe during January and July from the two runs. Interestingly, there appears to be a significant increase (of about 0.5 °C in the mean) in the summertime temperatures associated with changing S_{max}. Perhaps more interesting is the increase in the number of extremely warm July temperatures in the run with higher S_{max}. It appears that these result from an increase in incoming solar radiation despite very little change in the mean cloudiness. Apparently in the run with higher S_{max} Europe experiences more clear, sunny days.

Another region that shows significant differences between the models is the tropical Pacific. As seen in Fig. 3 the high S_{max} run is warmer to the south of the equator and colder on the equator. This results in exacerbating a well known problem with coupled models, namely the extension of the intertropical convergence zone into the eastern Pacific. The increased precipitation (Fig. 13a) is seen in all four seasons and also results in increases in high clouds (Fig. 13b) and local decreases in outgoing longwave radiation of up to 6 W m^{-2}
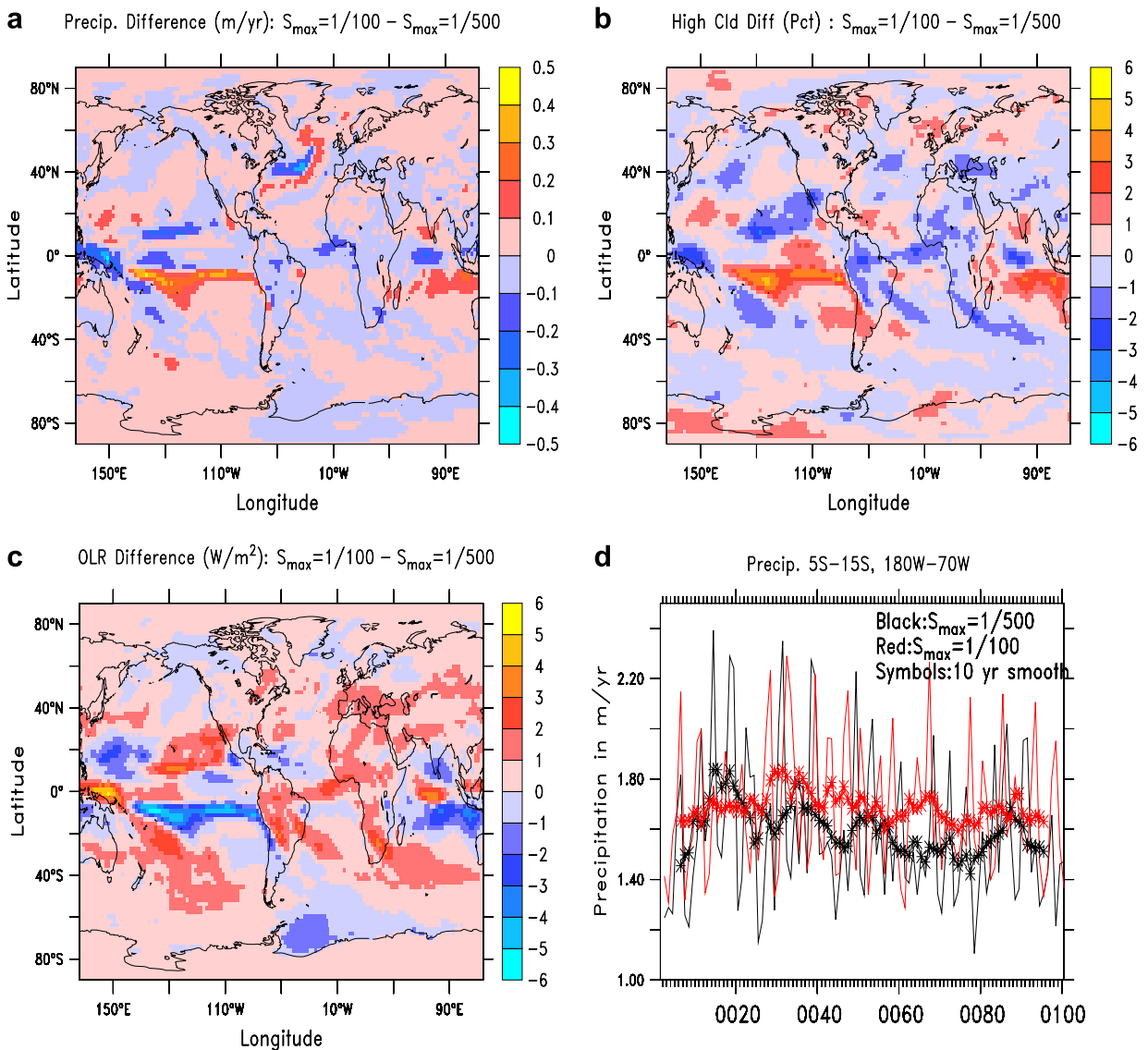

Fig. 13. Changes in the Pacific associated with increasing S_{max}. (a) Change in precipitation in m/yr. (b) Change in high cloud percentage. (c) Change in outgoing longwave radiation. (d) Annually averaged precipitation time series from the two simulations in the region from 180W to 80W and 5S to 15S.

(Fig. 13c). The signal is relatively robust interannually. While preliminary analysis (A. Wittenberg, personal communication) indicates that the change may impact the spectrum of temperature variability as well, full analysis of why this is the case is beyond the scope of this paper. In a coupled context the changes in Pacific atmospheric circulation also favor using a lower value of $S_{\max}$.

4. Discussion

Parameterizations of eddy-induced advection require an upper limit to be set on how large a transport can be associated with eddies in order to maintain numerical stability. We have shown that the details of how this limit is implemented, in particular the maximum value of the slope $S_{\max}$ can produce significant changes in the location, rates and processes responsible for vertical exchange. While the global RMS temperature and salinity errors are relatively insensitive to $S_{\max}$, Southern Ocean ventilation as diagnosed by the ideal age and heat uptake are much more strongly affected.

Probably the most important of these is the level of vertical exchange in the Southern Ocean. The properties of the abyssal ocean are primarily set by three sources, North Atlantic Deep Water, Circumpolar Deep Water, and Antarctic Intermediate Water. An important difference between these sources is their nutrient content – North Atlantic Deep Water is relatively depleted in nutrients such as phosphate relative to Circumpolar Deep Water. Chemical oceanographers refer to the nutrient content of water sinking into the abyss as the preformed content. Changes in the preformed carbon content of the deep ocean can have an important impact on atmospheric carbon dioxide (Marinov, 2005; Marinov et al., 2006). Toggweiler et al. (2006) have proposed that the change in atmospheric carbon dioxide between glacial and interglacial periods can be controlled by whether or not carbon sequestered in the deep ocean can escape through convective regions in the Southern Ocean. This paper suggests that details of the eddy parameterization can determine how well the process of opening and closing convective regions will be simulated otherwise "realistic" climate models.

Tuning a climate model involves considering many different processes and examining the many differences between models and observations. It is not our purpose in this paper to argue that one value of $S_{\max}$ is intrinsically superior to another. Instead, we wish to emphasize the details of how tapering is applied can alter the vertical structure of the response to changes in climate and may modulate important biogeochemical feedbacks. Unfortunately, this parameter is often chosen in an ad hoc manner and the value used is frequently not documented. This paper argues that climate modelers need to pay attention to these details, an argument bolstered by recent work by Danabasoglu et al. (2006) suggesting that such details play a more significant role in the NCAR ocean model. While the overall effect of $S_{\max}$ on traditional metrics for climate models (such as globally averaged SST error and hydrographic error) is relatively small in our simulation – it can change the overall radiative balance by about 0.5 W m^2 and can produce significant local changes in temperature and circulation. It is our hope that the ongoing Eddy-Mixed Layer Interaction Climate Process Team (http://cpt-emilie.org) will help to put better constraints on this process.

References

Conkright, M.E., Antonov, J., Baranova, O., Boyer, T.P., Garcia, H.E., Gelfeld, R., Johnson, D., Locarnini, R.A., Murphy, P.P., O'Brien, T.D., Smolyar, I., Stephens, C., 2002. NOAA Atlas NESDIS 42, World Ocean Database 2001. vol. 1: Introduction, US Govt. Printing Office, Washington, DC, pp. 160.
Cox, M., 1987. Isopycnal diffusion in a z-coordinate ocean model. Ocean Modelling 74, 1–5 (unpublished manuscripts).

Danabasoglu, G., Ferrari, R., McWilliams, J.C., submitted for publication. Sensitivity of an ocean general circulation model to a parameterization of near-surface eddy fluxes. J. Climate.

Davis, R.E., 2005. Intermediate-depth circulation of the Indian and South Pacific Oceans measured by autonomous floats. J. Phys. Oceanogr. 35, 683–707.

Delworth, T. et al., 2006. GFDL's CM2 global coupled climate models-Part 1: Formulation and simulation characteristics. J. Climate 19, 643–674.

Ferrari, R., McWilliams, J.C., submitted for publication. Parameterization of eddy fluxes at the ocean boundaries. J. Phys. Oceanogr.

Gent, P., McWilliams, J.C., 1990. Isopycnal mixing in ocean circulation models. J. Phys. Oceanogr. 20, 150–155.

Gent, P., Willebrand, J., McDougall, T.J., McWilliams, J.C., 1995. Parameterizing eddy induced transports in ocean circulation models. J. Phys. Oceanogr. 25, 463–474.

Gerdes, R., Koberle, C., Willebrand, J., 1991. The influence of numerical advection schemes on the results of ocean general circulation models. Climate Dynam. 5, 211–226.

GFDL Global Model Atmospheric Development Team, 2004. The new GFDL global atmosphere and land model AM2-LM2: evaluation with prescribed SST simulations. J. Climate 17 (24), 4641–4673.

Gnanadesikan, A., 1999a. A simple model for the structure of the oceanic pycnocline. Science 283, 2077–2079.

Gnanadesikan, A., 1999b. A global model of silicon cycling: sensitivity to eddy parameterization and dissolution. Global Biogeochem. Cycles 13, 199–220.

Gnanadesikan, A. et al., 2006. GFDL's CM2 global coupled climate models. Part 2: the baseline ocean simulation. J. Climate 19, 675–697.

Gnanadesikan, A., Slater, R.D., Gruber, N., Sarmiento, J.L., 2002. Oceanic vertical exchange and new production: a model-data comparison. Deep Sea Res. Part II 43, 363–401.

Gnanadesikan, A., Slater, R.D., Samuels, B.L., 2003. Sensitivity of water mass transformation and heat transport to subgridscale mixing in coarse-resolution ocean models. Geophys. Res. Lett. 30 (18), 1967. doi:10.1029/2003GL018036.

Gnanadesikan, A., Slater, R.D., Swathi, P.S., Vallis, G.K., 2005. The energetics of ocean heat transport. J. Climate 18, 2604–2616.

Gough, W.A., 1997. Isopycnal mixing and convective adjustment in an ocean model. Atmos. Ocean 25, 495–511.

Gough, W.A., Welch, W.J., 1994. Parameter space exploration of an ocean general circulation model using an isopycnal mixing parameterization. J. Marine Res. 52, 773–796.

Greatbatch, R.J., Lamb, K.G., 1990. On parameterizing vertical mixing of momentum in non-eddy resolving ocean models. J. Phys. Oceanogr. 20, 1634–1637.

Gregory, J.M., 2000. Vertical heat transports in the ocean and their effect on time-dependent climate change. Climate Dynam. 16, 501–515.

Griffies, S.M., 1998. The Gent–McWilliams skew-flux. J. Phys. Oceanogr. 28, 831–841.

Griffies, S.M., Gnanadesikan, A., Pacanowski, R.C., Larichev, V.D., Dukowicz, J.K., Smith, R.D., 1998. Isoneutral diffusion in a z-coordinate ocean model. J. Phys. Oceanogr. 28, 805–830.

Griffies, S.M., Gnanadesikan, A., Dixon, K.W., Dunne, J.P., Gerdes, R., Harrison, M.J., Rosati, A., Russell, J.L., Samuels, B.L., Winton, M., Zhang, R., 2005. Formulation of an ocean model for global climate simulations. Ocean Sci. 2, 45–79, www.ocean-science.net/os/1/45.

Griffies, S.M., Harrison, M.J., Pacanowski, R.C., Rosati, A., 2003. A Technical Guide to MOM 4, GFDL Ocean Group Technical Report No. 5, Princeton, NJ, NOAA Geophysical Fluid Dynamics Laboratory, pp. 295.

Griffies, S.M., Pacanowski, R.C., Schmidt, R.M., Balaji, V., 2001. Tracer conservation with an explicit free surface method for z-coordinate ocean models. Monthly Weather Rev. 129, 1081–1098.

Held, I.M., Larichev, V.D., 1996. A scaling theory for horizontally homogeneous baroclinic flow on a beta-plane. J. Atmos. Sci. 53, 946–952.

Ito,T., Marshall, J., Follows, M., 2004. What controls the uptake of transient tracers in the Southern Ocean? Global Biogeochem. Cycles 18(2), Art No. GB2021.

Karsten, R.H., Marshall, J., 2002. Constructing the residual circulation of the ACC from observations. J. Phys. Oceanogr. 32, 3315–3327.

Killworth, P.D., 1998. Eddy parameterization in large-scale flow. In: Chassignet, E.P., Verron, J. (Eds.), Ocean Modeling and Parameterization, NATO ASI Series. Kluwer Academic, pp. 253–268.

Killworth, P.D., 2001. Boundary conditions on quasi-Stokes velocities in parameterizations. J. Phys. Oceanogr. 31, 1132–1155.

Large, W., Danasbogulu, G., McWilliams, J.C., Gent, P.R., Bryan, F.O., 2001. Equatorial circulation of a global ocean climate model with anisotropic viscosity. J. Phys. Oceanogr. 31, 518–536.

Large, W., McWilliams, J.C., Doney, S.C., 1994. Oceanic vertical mixing: a review and a model with a nonlocal boundary mixing parameterization. Rev. Geophys. 32, 363–403.

Ledwell, J.R., Watson, A.J., Law, C.S., 1998. Mixing of a tracer in the pycnocline. J. Geophys. Res. 103, 21499–21530.

Levitus, S., Boyer, T.P., Conkright, M.E., O'Brien, T., Antonov, J., Stephens, C., Stathoplos, L., Johnson, D., Gelfeld, R., 1998. NOAA Atlas NESDIS 18, World Ocean Database 1998. vol. 1: Introduction, US Govt. Printing Office, Washington, DC, pp. 346.

Lin, S.J., 2004. A "vertically Lagrangian" finite-volume dynamical core for global models. Monthly Weather Rev. 132, 2293–2307.

Marinov, I., 2005. Controls on the air–sea balance of CO_2, Ph.D Dissertation, Princeton University.

Marinov, I., Gnanadesikan, A., Toggweiler, J.R., Sarmiento, J.L., 2006. The Southern Ocean biogeochemical divide. Nature 441, 964–967.

Matsumoto, K. et al., 2004. Evaluation of ocean carbon cycle models with data-based metrics. Geophys. Res. Lett. 31, L07303. doi:10.1029/2003GL018970.

McDougall, T.J., 1998. Three-dimensional residual mean theory. In: Chassignet, E., Verron, J.P. (Eds.), Ocean Modelling and Parameterization, NATO ASI Series. Kluwer Academic, pp. 269–302.

Mignone, B.K., Gnanadesikan, A., Sarmiento, J.L., Slater, R.D., 2006. Central role of Southern Hemisphere winds and eddies in modulating oceanic uptake of anthropogenic carbon dioxide. Geophys. Res. Lett. 33, L01604. doi:10.1029/2005GL024464.

Monterey, G., Levitus, S., 1997. Seasonal variability of mixed layer depth for the World Ocean. NOAA Atlas, NESDIS 14, Washington, DC, pp. 100.

Oschlies, A., 1999. On spurious interactions among a mixed layer model, convective adjustment and isopycnal mixing in ocean circulation models. Monthly Weather Rev. 127, 1920–1927.

Pacanowski, R.C., Gnanadesikan, A., 1998. Transient response in a z-level ocean model that resolves topography with partial cells. Monthly Weather Rev. 126, 3248–3270.

Pacanowski, R.C., Griffies, S.M., 1999. The MOM 3 Manual, Alpha Version, Technical Report, NOAA/Geophysical Fluid Dynamics Laboratory, Princeton, NJ, USA.

Redi, M.H., 1982. Isopycnal mixing by coordinate rotation. J. Phys. Oceanogr. 12, 1154–1158.

Rhines, P.B., Holland, W.R., 1979. A theoretical discussion of eddy-driven mean flows. Dynam. Atmos. Oceans 3, 289–325.

Rhines, P.B., Young, W.R., 1982. Homogenization of potential vorticity in planetary gyres. J. Fluid Mech. 122, 347–367.

Russell, J.L., Stouffer, R.J., Dixon, K.W., in press. Intercomparison of the Southern ocean circulations in IPCC coupled model control simulations. Journal of Climate.

Swallow, J.C., 1971. The Aries current measurements in the western North Atlantic. Phil. Trans. Roy. Soc. London, Ser. A 270, 451–460.

Toggweiler, J.R., Russell, J.L., Carson, S., 2006. Mid-latitude westerlies, atmospheric CO_2 and climate change during the Ice Ages. Paleoceanography 21, PA2005. doi:10.1029/2005PA001154.

Trenberth, K.E., Caron, J.M., 2001. Estimates of meridional atmosphere and ocean heat transports. J. Climate 14, 3433–3443.

Visbeck, M., Marshall, J., Haine, T., Spall, M., 1997. Specification of eddy transfer coefficients in coarse-resolution ocean models. J. Phys. Oceanogr. 27, 381–402.

Willey, D.A., Fine, R.A., Sonnerup, R.E., Bullister, J.L., Smethie, W.M., Warner, M.J., 2004. Global oceanic chloroflourocarbon inventory. Geophys. Res. Lett. 31, L1303. doi:10.1029/2003GL018816.

Winton, M., Hallberg, R.W., Gnanadesikan, A., 1998. Simulation of density-driven frictional downslope flow in z-coordinate ocean models. J. Phys. Oceanogr. 28, 2163–2174.